FUNDAMENTAL ANALYSIS OF RELATIVE PERMEABILITY AND HETEROGENEITY ON CARBON DIOXIDE STORAGE AND PLUME MIGRATION

by

Nathan David Moodie

A thesis submitted to the faculty of
The University of Utah
in partial fulfillment of the requirements for the degree of

Master of Science

Department of Civil and Environmental Engineering

University of Utah

May 2013

The University of Utah Graduate School

STATEMENT OF THESIS APPROVAL

The thesis of Nathan David Moodie

has been approved by the following supervisory committee members:

Brian J. McPherson	, Chair	**4 Mar 2013** Date Approved
Christine Pomeroy	, Member	**5 Mar 2013** Date Approved
Steven Burian	, Member	**4 Mar 2013** Date Approved

and by **Chris Pantelides**, Chair of the Department of **Civil and Environmental Engineering**

and by Donna M. White, Interim Dean of The Graduate School.

ABSTRACT

A critical aspect of geologic carbon storage, a carbon-emissions reduction method under extensive review and testing, is the ability to simulate multiphase CO_2 flow and transport. Relative permeability is a flow parameter particularly critical for accurate forecasting of multiphase behavior of CO_2 in the subsurface. Specifically, for clastic formations, small-scale (cm) bedding planes can have a significant impact on multiphase CO_2-brine fluid flow, depending on the relative permeability relationship assumed. Such small-scale differences in permeability attributable to individual bedding planes may also have a substantial impact on predicted CO_2 storage capacity and long-term plume migration behavior.

A major goal of this study was to evaluate and calibrate relative permeability models against experimental data to improve simulation capability. We analyzed previously-published laboratory-scale measurements of relative permeability of Berea sandstone, and developed a corresponding three dimensional simulation model of those measurements. The simulation model was created in the TOUGHREACT reactive transport simulator, and we elucidated best-fit relative permeability formulations to match the experimental data. Among several functions evaluated, best-fits between simulation results and experimental observations were achieved with a calibrated van Genuchten-Mualem formulation.

To extend the analysis to a more heterogeneous medium, we applied the best-fit relative permeability formulations to a new model of a small-scale Navajo Sandstone reservoir. The model was one cubic meter in size, with eight individual lithofacies of differing permeability, gridded to mimic small-scale bedding planes. For this model we

assumed that each lithofacies exhibits a random permeability field, resulting in a model with heterogeneous lithofacies. We then evaluated four different relative permeability functions to quantify their impact on flow results for each model, with all other parameters maintained constant. Results of this analysis suggest that CO_2 plume movement and behavior are significantly dependent on the specific relative permeability formulation assigned, including the assumed irreducible saturation values of CO_2 and brine. More specifically, different relative permeability formulations translate to significant differences in CO_2 plume behavior.

TABLE OF CONTENTS

ABSTRACT iii

LIST OF TABLES vi

LIST OF FIGURES vii

ACKNOWLEDGMENTS ix

Chapter

1 INTRODUCTION 1

2 LITERATURE SURVEY 3

3 CONCEPTUAL FRAMEWORK 6

3.1 Scope of Study 6
3.2 Relative Permeability Curve Fitting 7
3.3 Relative Permeability Curves 8
3.4 Core-scale Experiment 9
3.5 Bedform-scale Experiment 11
3.6 Effects of Model Domain Size on Model Predictions 13

4 RESULTS 19

4.1 Berea Sandstone Core Model 19
4.2 Navajo Sandstone Core Model 21
4.3 Vertical Migration Patterns of CO_2 22
4.4 Navajo Sandstone Bedform Model 22

5 CONCLUSION 33

REFERENCES 36

LIST OF TABLES

Table Page

1. Values for the regression analysis and root mean square error used to determine the best fit parameters for the Brooks-Corey and van Genuchten-Mualem functions....14

2. Relative permeability parameters used by TIOUGHREACT 15

3. Capillary pressure parameters used in TOUGHREACT....16

4. Fractional flows and the associated mass flow numbers used in each injection cell of the core flood models....16

5. Measured permeability data from the Devil's Canyon field site. The standard deviation illustrates that there is large variability in the permeability measurements, highlighting the limitations of the TinyPERM II™ in isolating single layers in the rock matrix....17

6. Total amount of supercritical and dissolved CO_2 predicted in the Berea Sandstone core model by each of the relative permeability curves....26

7. Total amount of supercritical and dissolved CO_2 predicted in the Navajo Sandstone core model by each of the relative permeability curves....28

8. Total amount of supercritical and dissolved CO_2 predicted in the Navajo Sandstone core model by each of the relative permeability curves....31

LIST OF FIGURES

Figure Page

1. Drainage CO_2 (solid circles) and water (open circles) experimental relative permeability data on Berea Sandstone from Krevor et al. (2012) fit to the Brooks-Corey curves.....14

2. Relative permeability of gas (2a) and water (2b) predicted by the Brooks-Corey and van Genuchten-Mualem functions compared to measured Berea Sandstone data.....15

3. Berea core mesh on the left and the Navajo core mesh on the right. The injection face is highlighted on the right of each model.....17

4. Navajo bedform mesh highlighting the position of each of the four active layer types and the 'dummy' layer at the bottom.....18

5. Results of four of the Berea sandstone simulations showing predicted mass of supercritical CO_2 in place for each relative permeability curve.....26

6. Results of four of the Berea sandstone simulations showing predicted mass of dissolved CO_2 phase in place for each relative permeability curve.....27

7. Results of four of the Navajo sandstone core simulations showing the predicted mass of supercritical CO_2 in place for each relative permeability curve 28

8. Results of four of the Navajo sandstone simulations showing predicted mass of dissolved CO_2 phase in place for each relative permeability curve.....29

9. Results of the 10kPa Navajo sandstone bedform model simulations showing the predicted mass of supercritical CO_2 in place for each of the relative permeability curves used in the heterogeneous (9a) and homogeneous (9b) models 29

10. Results of the 10kPa Navajo sandstone bedform model simulations showing the predicted mass of dissolved phase CO_2 in place for each of the relative permeability curves used in the heterogeneous (10a) and homogeneous (10b) models.....30

11. Results of the 100kPa Navajo Sandstone bedform model simulations showing the predicted mass supercritical of CO_2 in place for each of the relative permeability curves used in the heterogeneous (9a) and homogeneous (9b) models.....30

12. Results of the 100kPa Navajo sandstone bedform model simulations showing

the predicted mass dissolved phase of CO_2 in place for each of the relative permeability curves used in the heterogeneous (10a) and homogeneous (10b) models.....30

ACKNOWLEDGMENTS

I would like to acknowledge the contributions to my research from Brian McPherson, Si-Yong Lee, and the rest of the Carbon Science group. Without these gentlemen I would not have found such a unique niche in the study of carbon dioxide and water/brine multiphase fluid flow systems. I would like to thank them for guiding me in the direction of studying relative permeability relationships as they pertain to carbon sequestration research.

CHAPTER 1

INTRODUCTION

Published relative permeability data for binary systems of CO_2 and water/brine were sparse. Relative permeability data for the Navajo sandstone in particular have not been measured, or at least are not published. One of our research goals was to investigate the validity of using experimentally-derived relative permeability functions for a well-known formation, in this case the Berea sandstone, to calibrate a relative permeability function effective for modeling CO_2 behavior in a more heterogeneous formation. Because its prominence as a geologic CO_2 storage candidate, and because of its availability, we selected the Navajo sandstone as the more-heterogeneous formation for evaluation. Ideally, core flood experiments need to be conducted with the Navajo sandstone and relative permeability measured directly, at the time this article was written, we have just began such experiments. Upon completion of testing, we will evaluate the measured curves and compare to previously-published relative permeability values measured by Krevor et al. (2012). The specific focus of this study was to use simulations to investigate the effects of relative permeability on CO_2 plume movement and compare results of different relative permeability curves, in this context, to the Krevor et al. (2012) data.

Initially, numerical models of a Berea sandstone core and a Navajo sandstone core were created to mimic the relative permeability core flood experiments of Krevor et al. (2012). The relative permeability curves used in the numerical models were varied, and the response of the simulated CO_2 plume was quantified. Next, a small-scale bedform model of the Navajo Sandstone was developed, with the idea of mimicking Navajo

layering observed at the Devil's Canyon site in southern Utah. This site is an aboveground analog of what the Navajo sandstone is believed to be like at several potential sequestration sites in central Utah, such as Gordon Creek. To analyze how CO_2 behaves as it reaches lithofacies with varying permeability, a model was created that included four different lithofacies types, each with its own permeability values, or range of values in the case of heterogeneous simulations. We assigned Dirichlet boundary conditions on the top and bottom, and Neumann boundaries on the sides. A higher pressure was specified at the bottom to induce a pressure-driven upward flow across the model. The effect that relative permeability has on CO_2 flow and transport through lithofacies of different permeability was studied without the complications that injection can have on the model.

CHAPTER 2

LITERATURE SURVEY

Compared to intrinsic permeability, CO_2-brine and CO_2-brine-oil relative permeability data are scarce, and especially so for candidate CO_2 sequestration formations. Krevor et al. (2012) constructed relative permeability laboratory experiments on Berea sandstone. The experimental data were fit to the Brooks-Corey relative permeability function that was modified from the original formula put forth by Brooks and Corey in 1964. Krevor et al. (2012) cite this formula outlined by Dullien (1992) as the best fit for their experimental data. We compared Brooks and Corey's original formula to Dullien's formula and discovered an error in Dullien's equation with respect to the Brooks-Corey relative permeability function. The formula in Dullien (1992) doesn't match the formula developed by Brooks and Corey in their 1964 paper. The following two equations are Equation 1 from Dullien's book and Equation 2 from Brooks and Corey (1964); note that the equation from Dullien's book expresses the exponent (2+□)/□ on the outside of the parentheses of the third term, but in the original formula developed by Brooks and Corey (1964), this expression (2+□)/□ is on the inside of the parentheses, thus modifying S_{eff} directly. Bennion et al. (2007) produced laboratory measurements of potential seal rocks in the Alberta Basin, Canada and evaluated the relative permeability and capillary pressure curves for shale and anhydrites. They concluded that under normal injection pressures and reservoir conditions these formations act as seals over geologic time. Bennion et al. (2006) performed relative permeability and capillary pressure experiments on reservoir rock,

sandstone, and carbonate formations from the same area in Alberta, Canada. They expressed the importance of relative permeability and residual gas trapping in the pore spaces as important factors affecting injectivity and CO_2/acid gas mobility in a brine reservoir. Bennion et al. (2006) state the importance of knowing the capillary pressure curves for the seal rock, so that injection pressures can be kept below that threshold and CO_2 is not forced into the seal rock. Muller (2011) indicates the importance of relative permeability and capillary pressure data for flow simulations and the general lack of data available to modelers. He indicates that there is considerable complexity and difficulty in making such measurements (Muller 2011). Krevor et al. (2012) state that 'relative permeability and residual trapping characteristics' are highly variable, and are very difficult to estimate in the 'absence of direct observations'. They indicate that characterizing the difference in the petrophysical properties of the rock being studied would 'allow for a less arbitrary selection of generic multiphase flow parameters in simulation studies' when modeling of a specific rock type is not needed or wanted (Krevor et al. 2012). They also acknowledge that there have only been limited observations of systems that are relevant to CO_2 sequestration projects in deep saline geologic formations (Krevor et al. 2012).

Multiple authors have indicated the importance of using appropriate relative permeability curves and parameters for specific rocks under study when evaluating site specific numerical simulations (Krevor et al. 2012; Kumar et al. 2004; Lu et al. 2009; Doughty et al. 2001). It seems that most of the work done on CO_2 sequestration has used either generic relative permeability curves (Lu et al. 2009; White et al. 2001; Bielinski 2006; Kumar et al. 2004; Xu et al. 2005; Doughty et al. 2001) or do not mention relative permeability at all in their work (Xu et al. 2004; White et al. 2005). Some of these papers have been cited over 40 times (Doughty,Pruess 2004; White et al. 2005; Bielinski 2006) and some more than a hundred times (Kumar et al. 2004; Pruess et al. 2003; Pruess et

al. 1999; Xu et al. 2004, 2005) and are written by the foremost authorities in the their field. A notable exception is a paper by (Pruess et al. 2003) where they use the Corey and van Genuchten curves with parameters derived from actual relative permeability measurements from the Hanford formations in Washington as well as from specific soil types, such as loam, sand, silt. White et al. (2001) use the same Corey curve parameters that are used in this study to describe multiphase behavior in CO_2 reservoirs on the Colorado Plateau. The numerical models developed by our team suggest that the choice of relative permeability function and parameters may have a significant impact on CO_2 movement and phase behavior, even causing lithofacies within the target reservoir to act as a barrier to CO_2 flow under certain conditions.

CHAPTER 3

CONCEPTUAL FRAMEWORK

3.1 Scope of Study

A critical need for future CO_2 storage efforts in the western U.S. are robust relative permeability functions for simulating multiphase CO_2 flow in the Navajo sandstone. A goal of this project was to analyze the CO_2 plume response to different relative permeability curves and compare the results to existing experimental curves for Berea sandstone. Specifically, we quantified the disparity of flow fields among results of simulations that used different relative permeability functions.

For this study, the modeling effort was approached in two phases. The first step was to recreate the Krevor et al. (2012) core flood experiments using TOUGHREACT simulation models. A core model of the Berea sandstone was created to mimic the Krevor et al. (2012) experiment. Navajo sandstone parameters were applied to the same core model mesh to compare the difference another sandstone would have on the numerical model results. The objective was to quantify the magnitude of difference between the mass fluxes of CO_2 that each relative permeability curve predicts. Specified H_2O/CO_2 mixtures were injected into the core at a total flow rate of 15 mL/min to determine the fluid response to different relative permeability curves. This is the same flow rate used by Krevor et al. (2012) in their core flood experiments.

Next, we applied the same relative permeability curves to a small-scale bedform model of the Navajo sandstone. The bedform model more closely resembled the layering seen in the outcrops of Navajo sandstone. The models were created to mimic *in situ*

conditions at potential sequestration sites on the Colorado Plateau. With the final goal of determining the validity of using the Krevor's parameters as a proxy for the unknown Navajo sandstone relative permeability parameters—or if other curves investigated yielded more consistent results.

3.2 Relative Permeability Curve Fitting

To determine what function would be a fair representation of the experimental relative permeability data for Berea sandstone, we created a single cell "batch" model, assigned specific CO_2 mass fractions, and plotted the relative permeability data against the Berea sandstone experimental data. The experimental relative permeability curve for the Berea sandstone was digitized from data in the Krevor et al. (2012) paper. Figure 1 shows the experimental drainage CO_2 (solid circles) and water (open circles) data fit to the Brooks-Corey curves for Berea Sandstone from Krevor et al. (2012). Using these experimental data points (water saturation values), we calculated the corresponding individual relative permeability values for the Brooks-Corey formula presented by Krevor et al. (2012) and a van Genuchten-Mualem function chosen by our team.

A fundamental regression analysis determined the best-fitting parameters for each of the curves used in the subsequent models. The root mean square error (RMSE) values were calculated and the best "fit" was chosen to represent the experimental curve in our simulations. From the values given in Table 1 it was clear that either function will accurately reflect the experimental values and yield an acceptable curve for our simulations. The difference in RMSE and R^2 between the Brooks-Corey curve and the fitted van Genuchten-Mualem curve was close enough that the fitted van Genuchten-Mualem function was chosen for the core simulations. TOUGHREACT does not have the Brooks-Corey relative permeability function as part of the simulation package making the van Genuchten-Mualem function a convenient choice. This relative permeability

curve was called the 'Krevor' curve and Fig. 2a and 2b present the regression analysis done to justify using the van Genuchten-Mualem function to create this curve.

3.3 Relative Permeability Curves

In this study four different relative permeability curves were investigated. The 'Krevor' curve became the 'base curve'. Three additional curves were used in this study, a linear curve, a second van Genuchten curve, and a Corey's curve. These three additional curves were not fitted to the Berea sandstone data but used to evaluate the effect of differing relative permeability curves on simulation result. Each of these curves was derived from one of the following functions; the linear functions, the Corey's curves, and the van Genuchten-Mualem model that are in TOUGHREACT. The second van Genuchten-Mualem curve was derived from values used in the TOUGH2 manual (Pruess et al. 1999). The linear function and the Corey's curve were used for the third and fourth curves evaluated. The parameters used in these curves were adapted for this study from values found in the TOUGH2 manual (Pruess et al. 1999). Our group has used the linear function and the van Genuchten-Mualem model to evaluate different aspects of CO_2 sequestration including storage potential and plume migration in the Navajo sandstone. The Corey's curve has not been used by anyone in our group until this study and was chosen for this reason. Table 2 has the parameters used for each of the functions.

A fifth relative permeability curve was evaluated using the Brooks-Corey function presented in Brooks and Corey (1964) and the parameters from Krevor et al. (2012). The Brooks-Corey function showed a very good fit with Krevor's experimental curve, as expected. But when the code was programmed into TOUGHREACT, we encountered numerical stability issues forcing us to abandon this function for the study. At this time the problem is being investigated.

Capillary pressure curves were also assigned to each of the simulations based on the relative permeability function used in each case. The van Genuchten-Mualem model and linear function both explicitly have capillary pressure functions associated with them, but the Corey's function does not. For the Corey's curve, a linear capillary pressure function was used. Table 3 summarizes study parameters.

3.4 Core-scale Experiment

The Krevor et al. (2012) core-flood experiment, we parameterized eleven specific H_2O/CO_2 mixtures for each of the four relative permeability curves studied. Each simulation had a specific ratio of H_2O to CO_2, with a total flow rate of 15 mL/min. This was accomplished by injection of both H_2O and CO_2 at specified mass flow rates along the injection face of the core. Each model had an initial simulation run with 100% H_2O to set up the initial pressure and temperature profile, which was then used as the initial conditions for the subsequent ten simulations. Table 4 shows the H_2O/CO_2 mixtures and mass flow rates used in the simulation.

To simulate a core flood experiment, a numerical model of a 2 inch × 4 inch sandstone core was gridded. The model was evaluated horizontally to match the experimental setup outlined by Krevor et al. (2012). The model includes 193 injection cells on one face and an infinite-volume boundary on the other face, with no-flow boundaries elsewhere. The model domain had a total of 6,692 cells (see Figure 3 for the Berea and Navajo core models). The pressure and temperature were set to 9MPa and 50°C, respectively. Pure water and CO_2 are the two working fluids used in the simulations. All core simulations were run for a simulation period of four hours. The Berea sandstone model in Figure 3 was homogeneous with a set permeability of 300 mD, to match the Berea core used by Krevor et al. (2012) in their study. The Navajo sandstone model in Figure 3 has 13 individual zones modeled after four lithofacies types, with each lithofacies being

homogeneous. The four distinct lithofacies modeled were the grain flow (GF00x), wind ripple lamina (WRL0x), course lag (CL00x), and wind ripple lamina/grain flow (WRLGx). Table 5 has the permeability values for each of the lithofacies used in the model.

These four lithofacies represent the small-scale heterogeneities in the Navajo sandstone outcrops observed at Devil's Canyon, Utah during field research conducted in the summer of 2011 (Allen et al. 2011). We considered this site an aboveground analog of what the Navajo sandstone is believed to be like at several potential sequestration sites in central Utah, such as the Gordon Creek field near Price, Utah. The permeability values used in each of the lithofacies were an average of the measured permeability, as measured by Allen et al. (2011). Permeabilities for each layer were measured *in situ* using a TinyPERM II™ air permeameter.

Large variability in measured values was observed for each layer in the field, due to the relatively large diameter, about 9 mm, of the TinyPERM II™ compared to the millimeter scale of the individual lithofacies observed in the outcrop. Also, the outcrop exhibited more than the four lithofacies used in the models. The four lithofacies used in the models represent the most common types of layering observed in the outcrop. With such a wide variability in the measured data, the permeability values used in the model can only be thought of as an estimation of the common lithofacies seen in the outcrop. Many factors could render these values inaccurate, such as the effects of weathering has on the permeability of the rock at the surface, or the difference in scale between the TinyPERM II™ orifice and the individual lithofacies.

3.5 Bedform-scale Experiment

The small-scale Navajo bedform model was built to represent an approximate one-meter cube of the eolian Navajo sandstone that is a potential target for sequestration in

central Utah and the broader Colorado Plateau. The Navajo sandstone at the Gordon Creek field near Price, Utah, is present at a depth of 2560 m below the surface, and accordingly, we assigned a hydrostatic initial condition of 25.7 MPa. The temperature is estimated to be 67.8°C at this depth, using an extrapolated linear temperature gradient based on measured values within the deeper, Permian-aged White Rim formation that yields a temperature gradient of 22.5°C/km (Chidsey,Chamberlain 1996). The brine has a salt concentration of 0.36% NaCl, typical for the Navajo sandstone in the area surrounding Gordon Creek (Hood,Patterson 1984).

Using this information, a centimeter-scale three-dimensional bedform model was built, using TOUGHREACT (with its ECO2h equation-of-state module) to model multiphase flow of CO_2 in brine. The bedform model consists of the same eolian Navajo sandstone rock properties as the core model. The approach was to simulate CO_2 flow through this model under a vertical pressure gradient, while varying the relative permeability curves used, and study the model's response. This model used the same four relative permeability curves used in the core models and described above. Table 2 summarizes the relative permeability parameters used in this analysis and Table 3 has the capillary pressure parameters. The specific relative permeability equations are given in the TOUGH2 Users Manual (Pruess et al. 1999).

The Navajo bedform model domain (grid) is 100 cm × 100 cm × 88 cm in the x, y, z directions; Figure 4 depicts the mesh. It consists of the same four layer types used in the Navajo Sandstone core model patterned after observed layering at Devil's Canyon. The grain flow layers (GF001) makes up the bulk of the model with a combined volume of 0.8 m^3. The two wind ripple lamina / grain flow layers (WRLG2) have a combined volume of 0.04 m^3, the wind ripple lamina layer (WRL03) has a volume of 0.02 m^3, and the course lag layer (CL004) has a volume of 0.02 m^3. An "Inactive" layer was added to the bottom of the model to act as a constant source of CO_2 at an assigned mass fraction of 0.50. The

"inactive" elements permit specific conditions, such as constant head (pressure), temperature, and fluid content, to be fixed, and these conditions will affect the model but are not included in the mass or energy balance equations (Pruess et al. 1999). This approach essentially gives the model a boundary condition with an unlimited source of fluid that is 50% CO_2. The inactive layer was also assigned as a constant head boundary, and assigned higher pressure then the rest of the model. This created a vertical head gradient that caused the CO_2 to flow upward through the model without the need for injection cells and the associated issues that can arise, such as very high pressures at the injection site. Greater control of the pressure regime being studied is also made easier. Two different pressure regimes were evaluated in this study; one with a 10 kPa □P from top to bottom, and one with a 100 kPa □P, ultimately driving fluid vertically from bottom to top. The top layer was also assigned as constant head and pressure boundary equivalent to 25.701 MPa, allowing the CO_2 to flow to and out of the top of the model. The four sides were assigned no-flow boundaries. In sum, this set of boundary conditions allowed CO_2 to migrate upwards through the reservoir to mimic vertical flow induced by the high pressure of an injected plume, without having to simulate the actual injection blocks.

Each of the two pressure regimes was applied to a homogeneous and a heterogeneous version of the model. This in effect created four different Navajo bedform models. All of the models consisted of the same four bedding planes, shown in table 5, as the Navajo core model; the grain flow, course lag, wind ripple lamina, and wind ripple lamina/grain flow. In the homogeneous models each of the four bedding planes have a homogeneous permeability field within. The heterogeneous models used TOUGH2's ability to create a random heterogeneous permeability field for each of the bedding plane types modeled. The heterogeneous models used the linear permeability modifier to create the random permeability fields, creating completely heterogeneous models. After

a number of initial simulation runs with different times, including one trial with 1000 years of simulations time, a 3-hour simulation was determined to be sufficient for the analysis planned. The results indicated that the model reached near steady state after about one hour and reaches complete equilibrium within 11.5 years. In the interest of saving computational time, a 3-hour simulation time was used.

3.6 Effects of Model Domain Size on Model Predictions

The size of the model domain that is chosen can have an effect on the results. The core flood model domain size was dictated by the core flood experiment being modeled. The Navajo bedform model domain size was a more arbitrary selection based on balancing computational time with grid resolution. So to get an idea if there was any noticeable effect to using a small scale model domain, a third model was created. This model was a larger version of the Navajo bedform model, double the size in the x-y-z direction, 200 cm x 200 cm x 178 cm. The layering was still patterned after the Navajo bedform model with alternating layers of grain flow and the thinner three layers. The simulation was run with the Krevor curve and the 100kPa □P heterogeneous model parameters. What was observed from the model outcome showed that there was not a noticeable difference in the CO_2 plume movement and saturation values when compared to the Navajo bedform model. The boundary effects did not have a noticeable impact on the model predictions. This gave us confidence that the influence of the boundary conditions on the Navajo bedform model results are negligible.

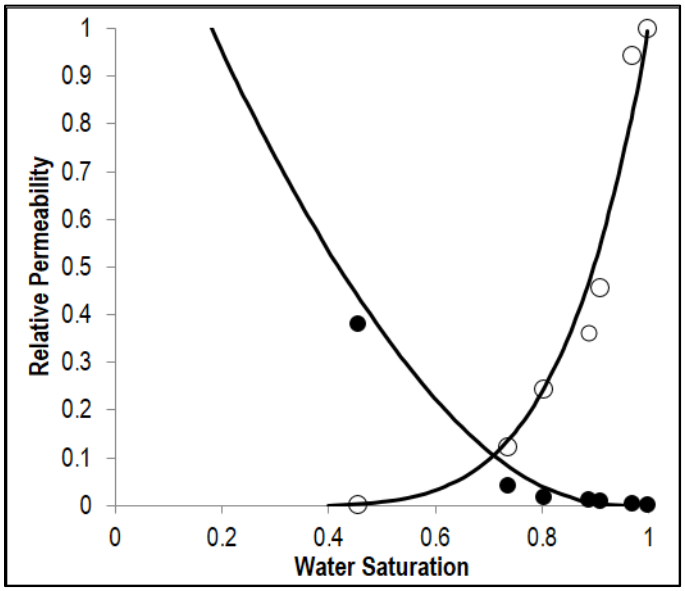

Figure 1. Drainage CO_2 (solid circles) and water (open circles) experimental relative permeability data on Berea Sandstone from Krevor et al. (2012) fit to the Brooks-Corey curves (solid lines).

Table 1. Values for the regression analysis and root mean square error used to determine the best fit parameters for the Brooks-Corey and van Genuchten-Mualem functions.

Root Mean Square Error and Regression Analysis		
	brooks-corey 1964	van Genuchten
RMSE - Gas	0.023	0.011
RMSE - Water	0.067	0.093
R^2 - Gas	0.997	0.987
R^2 - Water	0.975	0.963

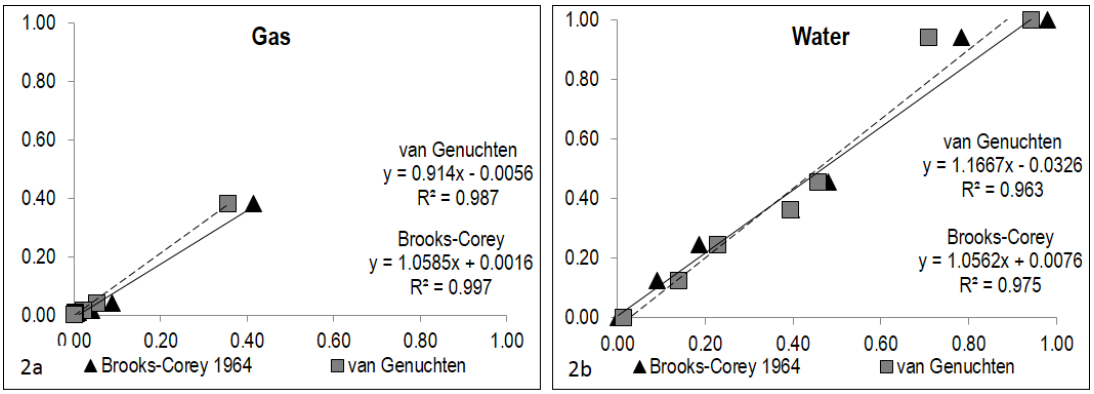

Figure 2. Relative permeability of gas (2a) and water (2b) predicted by the Brooks-Corey and van Genuchten-Mualem functions compared to measured Berea Sandstone data. The y-axis is the experimental relative permeability data from Krevor et al. (2012) and the x-axis is the predicted relative permeability data from the functions listed.

Table 2. Relative permeability parameters used in TOUGHREACT.

Relative Permeability Parameters				
	Linear Function	Corey's Curve	van Genuchten - Pruess[1]	van Genuchten - Krevor[2]
Lambda - λ	n/a	n/a	0.457	0.67
Water i-sat. (S_{rs})	0.2	0.3	0.15	0.2
Gas sat. (S_{gs})	1	n/a	n/a	n/a
Water sat. (S_{ls})	1	n/a	1	1
Gas i-sat. (S_{gr})	0.05	0.05	0.1	0.05

1 Pruess et al. 1999

2 Values are modified to match the Berea sandstone as measured by Krevor et.al. (2011)

Table 3. Capillary pressure parameters used in TOUGHREACT

Capillary Pressure Parameters			
	Linear Function	van Genuchten - Pruess[1]	van Genuchten - Krevor[2]
CP(1)	1000000	0.457 - λ	0.67 - λ
CP(2)	0.2	0.0 - S_{lr}	0.15 - S_{lr}
CP(3)	0.9	$5.105e^{-4}$ - $1/P_0$	$4.0e^{-4}$ - $1/P_0$
CP(4)	n/a	$1.0e^{7}$ - P_{max}	$1.0e^{7}$ - P_{max}
CP(5)	n/a	1 - S_{ls}	1 - S_{ls}

1 Pruess et al. 1999

2 Values are modified to match the Berea sandstone as measured by Krevor et.al. (2012)

Table 4. Fractional flow rates of H_2O and CO_2 and the associated dual injection rates used in each injection cell of the core flood models.

Core Scale Model - Injection Rates			
Fractional flow		Mass flow per cell (Kg/s)	
		COM1	COM3
H_2O	CO_2	H_2O	CO_2
1	0	1.28E-06	0.00E+00
0.95	0.05	1.22E-06	1.81E-08
0.9	0.1	1.16E-06	3.63E-08
0.8	0.2	1.03E-06	7.25E-08
0.7	0.3	8.99E-07	1.09E-07
0.5	0.5	6.42E-07	1.81E-07
0.3	0.7	3.85E-07	2.54E-07
0.2	0.8	2.57E-07	2.90E-07
0.1	0.9	1.28E-07	3.26E-07
0.05	0.95	6.42E-08	3.45E-07
0	1	0.00E+00	3.63E-07

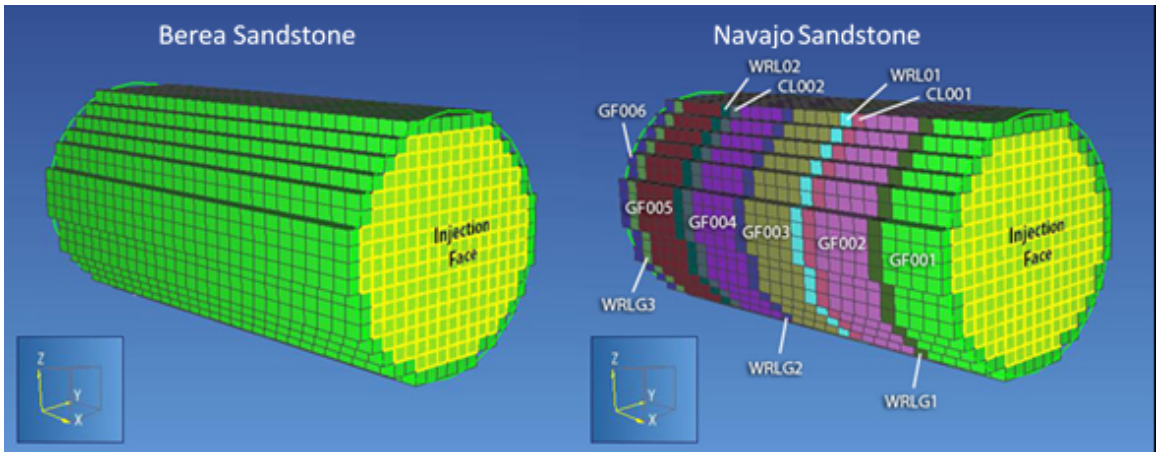

Figure 3. Core flood model mesh; the Berea core on the left and the Navajo core on the right. The injection face is highlighted on the right of each model. The individual layers in the Navajo mesh are the Grain Flow (GF001-GF005), Wind Ripple Lamina/Grain Flow (WRLG1-WRLG3), Wind Ripple Lamina (WRL01-WRL02), and Course Lag (CL001-CL002).

Table 5. Measured permeability data from the Devil's Canyon field site. The standard deviation illustrates that there is large variability in the permeability measurements, highlighting the limitations of the TinyPERM II™ in isolating single layers in the rock matrix.

Layer Data for Navajo Sandstone					
Layer Name	TOUGH code	Permeability		Standard deviation	
		mD	m^2	mD	m^2
Wind ripple lamina	WRL03	280	2.7636E-13	119	1.17E-13
Wind ripple lamina/Grain flow	WRLG2	388	3.8296E-13	171	1.69E-13
Grain flow	GF001	560	5.5272E-13	311	3.06E-13
Course lag	CL004	5346	5.2765E-12	2329	2.30E-12
Dummy	DUM05		1.00E-12	n/a	n/a

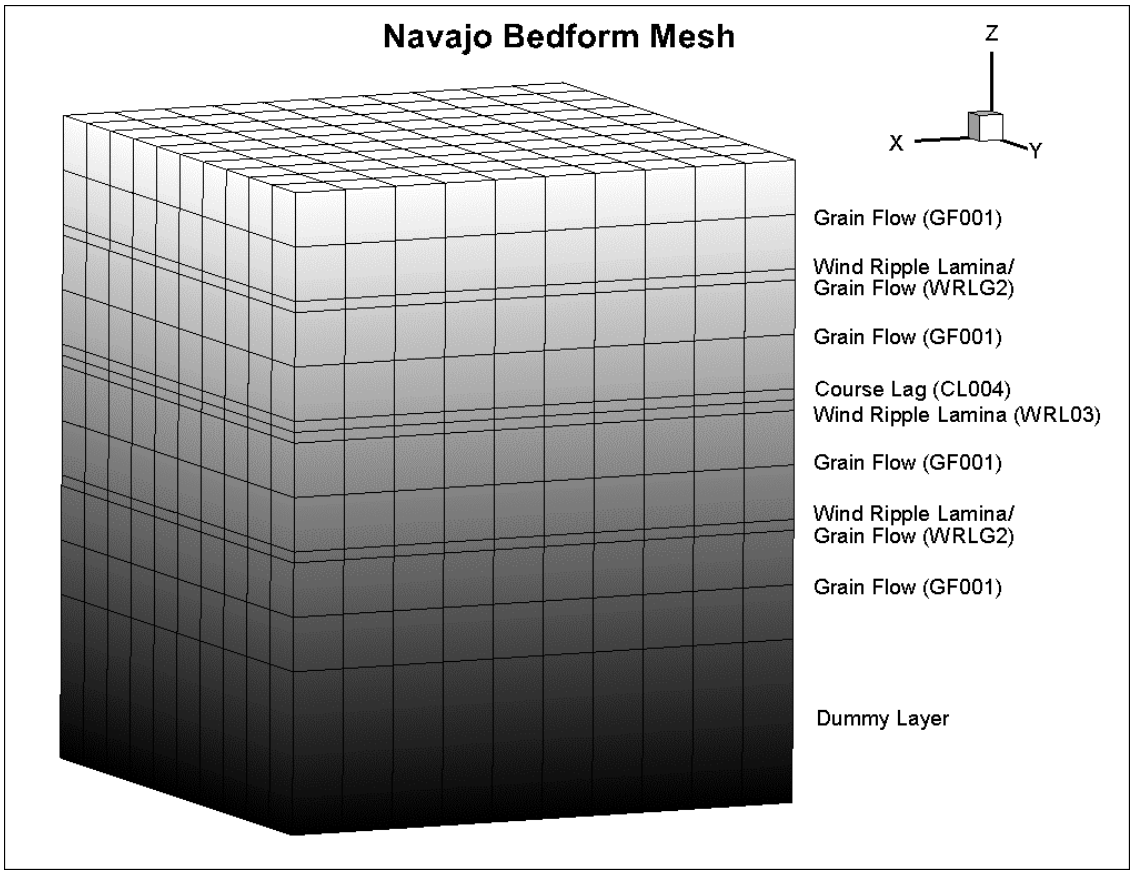

Figure 4. Navajo bedform mesh highlighting the position of each of the four active layer types, the Grain Flow, Wind Ripple Lamina, Wind Ripple Lamina/Grain Flow, Course Lag, and the 'dummy' layer at the bottom.

CHAPTER 4

RESULTS

For the Berea core model simulations, the van Genuchten-Mualem model with Krevor et al. (2012) parameters were used as a "standard" or base model simulation, and the results of that simulation were used as the basis of comparison. With the understanding that experimental Berea and Navajo sandstone curves were likely different, the same approach was used for the Navajo core model. But even with not having an experimental curve for the Navajo sandstone, we still wanted to explore what magnitude of variation in predicted CO_2 migration patterns might occur for the various relative permeability curves.

4.1 Berea Sandstone Core Model

The Berea core model simulations showed some useful insights regarding the predicted amount of supercritical CO_2 present as different relative permeability curves were used. Specifically, we compared results of simulations that used the different relative permeability formulations considered in this study, namely the formulation by Krevor et al. (2012), or what we will call the Krevor curve, and the formulation published by Pruess et al. (1999), hereafter called the Pruess curve, the original Corey's curve (Corey 1954) formulation, hereafter called the Corey curve, and a simple linear formulation. If between 20% and 80% CO_2 is flowed through the model, the Pruess and Krevor curve results predicts the most supercritical CO_2 and the linear curve the least. As the fractional flow of CO_2 is increased, the curve using the Pruess parameters predicts an

ever-decreasing amount of CO_2 compared to the "base case" Krevor curve. The Pruess curve goes from predicting about 1.2% more supercritical CO_2 for the 20% CO_2 fractional flow trial to predicting about 5.5% less for the 80% CO_2 trial. At a 50% CO_2 fractional flow the Pruess curve predicts only 1.1% more supercritical CO_2 and the mass flux curves (Figure 5b) match indicating that these two curves essentially predict the same amount of supercritical CO_2 for this given pressure regime. At the 100% CO_2 fractional flow trial the Pruess curve shows about 8% less supercritical CO_2 than the Krevor curve, indicating that only at the highest saturations of supercritical CO_2 was there any appreciable difference in predicted supercritical CO_2 between the Pruess and Krevor curves. The linear curve and the Corey curve consistently predicted 40-70% less mass of supercritical CO_2, with the liner curve being the most conservative. At the 20% CO_2 fractional flow trial the Corey curve predicted 1.3 grams of supercritical CO_2, about 47% less than what was predicted by the "base case" Krevor curve. The linear curve for the same CO_2 concentration predicted only 0.6 grams of supercritical CO_2, 74% less than the Krevor curve. At the 50% CO_2 fractional flow trial the Corey curve predicts 64% less supercritical CO_2 than the Krevor curve while the linear curve predicts over 80% less supercritical CO_2. This trend continues with the 80% and 100% CO_2 fractional flow trials with the Corey and linear curves predicting between 55% and 85% less supercritical CO_2 than the Krevor curve. Table 5 shows the total amount of predicted supercritical CO_2 by each of the relative permeability curves. Figure 5a to 5d illustrate that the Krevor and Pruess curves have a similar shape and the Corey and linear curves have a similar shape, but a big difference is apparent between those two groups. Figure 5a-5d also show the predicted amount of supercritical CO_2 for each of the curves. As summarized by Table 6, there is almost no difference in the predicted amount of dissolved CO_2 between the different relative permeability curves used in this study. This indicates

that the choice of relative permeability curves does not have an appreciable impact on predicted amounts of dissolved CO_2 in the same way it does for the supercritical phase. This is to be expected because Henry's Law predicts the solubility of CO_2 in brine, not the relative permeability function. The linear curve is the only curve that predicts any noticeable difference in dissolved phase CO_2, consistently predicting 5% to 9% more dissolved CO_2 than the Krevor curve. This could be due to changes in the pressure regime that the linear relative permeability function causes. Figures 6a to 6d illustrate this trend.

4.2 Navajo Sandstone Core Model

The Navajo core model simulations exhibited a very different response to the specific relative permeability curves assigned, as compared to the Berea model. The Pruess curve consistently predicts about 65% more supercritical CO_2 than the Krevor curve. Only at 100% CO_2 does the Pruess curve become closer to the Krevor curve in its prediction, but still predicting 32% more supercritical CO_2. Interestingly the linear curve was within a couple of percent of the Krevor curve predictions for the 50% CO_2 and 80% CO_2 trials and predicts 25% more supercritical CO_2 for the 20% CO_2 trial. When the fractional flow of CO_2 is increased to 100% the linear curve exhibits 65% less CO_2 flow through the model than the Krevor curve. The Corey curve consistently predicts more CO_2 movement through the model than the Krevor curve in all trials except the 100% CO_2 fractional flow trial by between 150%, for the 20% CO_2 trial, and 35%, for the 80% CO_2 trial. When the fractional flow of CO_2 is increased to 100% the Corey curve exhibits a 48% lower amount of CO_2 then the Krevor curve. Figure 7a to 7d illustrate this trend and Table 7 shows the total amount of CO_2 that flowed through the model for each of the relative permeability curves used. This is very different then what is predicted in the Berea Sandstone core model, where the Corey and linear curves consistently predicted less of the supercritical

phase then the Krevor curve while the Pruess curve followed the Krevor curve very closely in its predictions.

4.3 Vertical Migration Patterns of CO_2

The Krevor, Pruess, and linear relative permeability curves used in this study exhibited vertical migration effects that appear to be related to the buoyancy of CO_2 in water. The simulations results for most of the trials show gas saturation was higher along the top of the core models. This could be due to the differences in density of supercritical CO_2 and water leading to slightly higher concentrations along the top of the model. The Corey's curve did not exhibit these effects and ongoing work is being done to investigate this phenomena.

4.4 Navajo Sandstone Bedform Model

Applying the same relative permeability curves to the Navajo sandstone bedform model (Figure 4) yielded results quite different from either of the core model simulations. As with the core scale simulations the Krevor curve was used as the base case to which the rest of the relative permeability curves were compared against. The rational for using the Krevor curve as the "base case" was that it was calibrated against an experimental relative permeability curve. Understanding the disparity between the Krevor curve and the other relative permeability curves examined was the focus of this study.

4.4.1 10kPa Simulations

Four suites of simulations were done using the Navajo bedform model to examine the effect the choice of relative permeability curve has on the mass of CO_2 predicted. In the 10kPa heterogeneous simulation the linear curve exhibits the greatest disparity when

compared to the Krevor curve results, exceeding the “base case” mass of supercritical CO_2 phase by more than 460% and the dissolved phase CO_2 by 76%. Simulations reflected a similar result for the linear curve in the 10kPa homogeneous simulation, exceeding the “base case” mass of the supercritical phase by 290% and the dissolved phase by 43%. We interpreted these results to indicate that both supercritical CO_2 and dissolved CO_2 moves rapidly through the model but then reaches a saturation plateau at about five minutes into the simulation. After this point in time almost no increase in the mass of CO_2 moving through the model occurs, suggesting that under this pressure regime CO_2 saturation will not increase in the model.

At the 10kPa pressure regime for both the heterogeneous and homogeneous models the Pruess and Corey curves show a CO_2 movement that is similar to the Krevor curve but very different from what the linear curve shows. These two curves predict a much smaller amount of supercritical CO_2 flowing into the model, but still 50% to 90% more than is predicted by the “base case” Krevor curve. Table 8 show the total amount of CO_2 predicted by each of the relative permeability curves for all for models.

For the dissolved phase the Pruess curve almost matches the Krevor curve, within 2% for the heterogeneous model and 5% for the homogeneous model. The Corey curve predicts 26% less of the dissolved phase in the heterogeneous model and 15% less dissolved phase in the homogeneous model then the Krevor curve. What really stands out in contrast to the linear curve predictions is that for the Corey curve no supercritical CO_2 migrates upward into the Wind Ripple Lamina layer (WRL03) indicating that for the time simulated the WRL03 layer is acting as a barrier or seal not allowing the CO_2 to move into the upper part of the model. Both the Krevor and Pruess curves show a similar result as the Corey curve except that only a very small amount of supercritical phase moves into the WRL03 layer, on the order of 10^{-2} to 10^{-3} kg and only at the very end of the simulation. Figures 9a and 9b show the predicted mass of supercritical CO_2 in the

model. The dissolved phase shows the same trend as the supercritical phase for the Krevor, Pruess, and Corey curves. Only very small amounts of dissolved CO_2 are present in the model until the very end of the simulation, on the order of 10^{-18} to 10^{-19} kg. Figures 10a and 10b show the predicted mass of the dissolved phase CO_2 present in the models.

4.4.2 100kPa Simulations

The 100kPa simulations show a very different phase behavior compared to the 10kPa simulations. As observed in the 10kPa simulations, the linear curve results in rapid movement of the supercritical CO_2 through both the heterogeneous and homogeneous models, reaching a saturation plateau after about five minutes. Increases in supercritical CO_2 content cease at this stage. The dissolved phase response, in contrast, continues to increase until the end of the simulation. We believe this is due to the supercritical CO_2 continuing to encounter and dissolve into the surrounding water phase as it flow through the model. As such, while CO_2 continues to dissolve from the supercritical phase, the total concentration of the supercritical phase remains the same because relative permeability conditions (and therefore flow of supercritical CO_2) have reached a steady-state condition with the amount of dissolution over time. The Krevor curve acts similarly to the linear curve in the supercritical CO_2 phase behavior but with a longer time before it reaches a saturation plateau. The heterogeneous model with the Krevor curve is within 5% of the linear curve and for the homogeneous model within 3%. Table 8 illustrates this trend. The Pruess and Corey curves produce results similar to each other but quite differently from the Krevor curve results, especially in their supercritical phase CO_2 predictions. The Pruess results show 58% more supercritical CO_2 than the Krevor curve in the heterogeneous simulation and 60% more supercritical CO_2 in the homogeneous model. The Corey curve exceeds the “base case” mass predictions of supercritical CO_2 in both the heterogeneous and the homogeneous model by about 79%. Figures 11a and 11b

illustrate this trend in supercritical CO_2. The dissolved phase for both the heterogeneous and homogeneous 100kPa models act quite differently than in the 10kPa models with the Krevor curve consistently predicting the most CO_2. All relative permeability curves show a continuous flow of dissolved phase through the models, even the linear curve that in the 10kPa models reached a saturation plateau. Figures 12a and 12b illustrate this trend.

One of the most interesting results from the bedform model simulations was that for the 10kPa pressure differential models, heterogeneous and homogeneous, both phases of CO_2 become essentially trapped below the lower permeability wind ripple lamina lithofacies, and only a small amount of CO_2 migrates into the upper half of the models. Only the linear curve acts differently, reaching a saturation plateau of both supercritical and dissolved phase CO_2. When the pressure differential is increased to 100kPa both phases of CO_2 begin to flow through the model except for the linear curve. The liner curve shows the supercritical phase reaching a saturation plateau, similar to the 10kPa simulation, but the dissolved phase continues to increase throughout the simulation time.

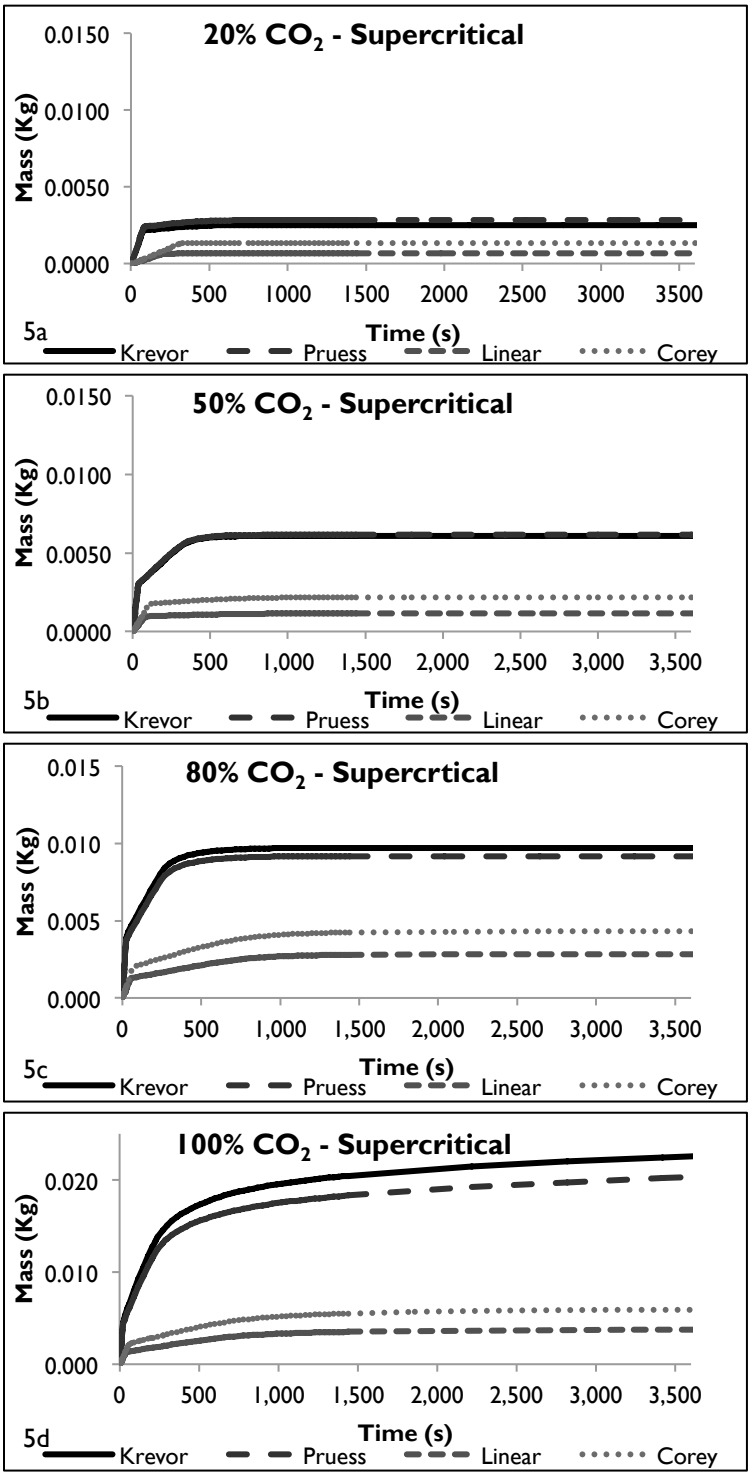

Figure 5. Results of four of the Berea sandstone simulations showing predicted mass of supercritical CO_2 in place for each relative permeability curve. 5a shows the 20% CO_2/80% H_2O simulation, 5b shows the 50% CO_2/50% H_2O simulation, 5c shows the 80% CO_2/20% H_2O simulation, and 5d shows the 100% CO_2 simulation.

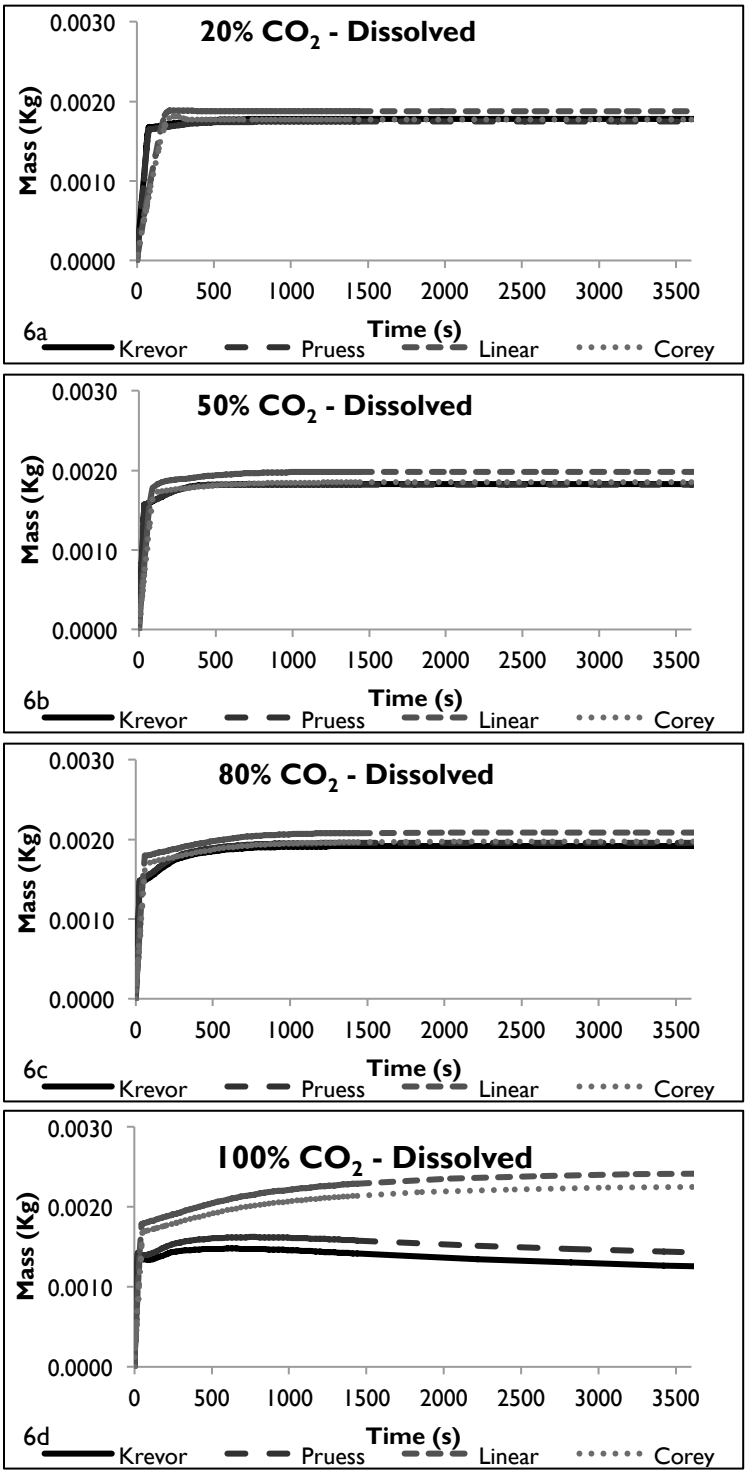

Figure 6. Results of four of the Berea sandstone simulations showing predicted mass of dissolved CO_2 phase in place for each relative permeability curve. 6a shows the 20% CO_2/80% H_2O simulation, 6b shows the 50% CO_2/50% H_2O simulation, 6c shows the 80% CO_2/20% H_2O simulation, and 6d shows the 100% CO_2 simulation.

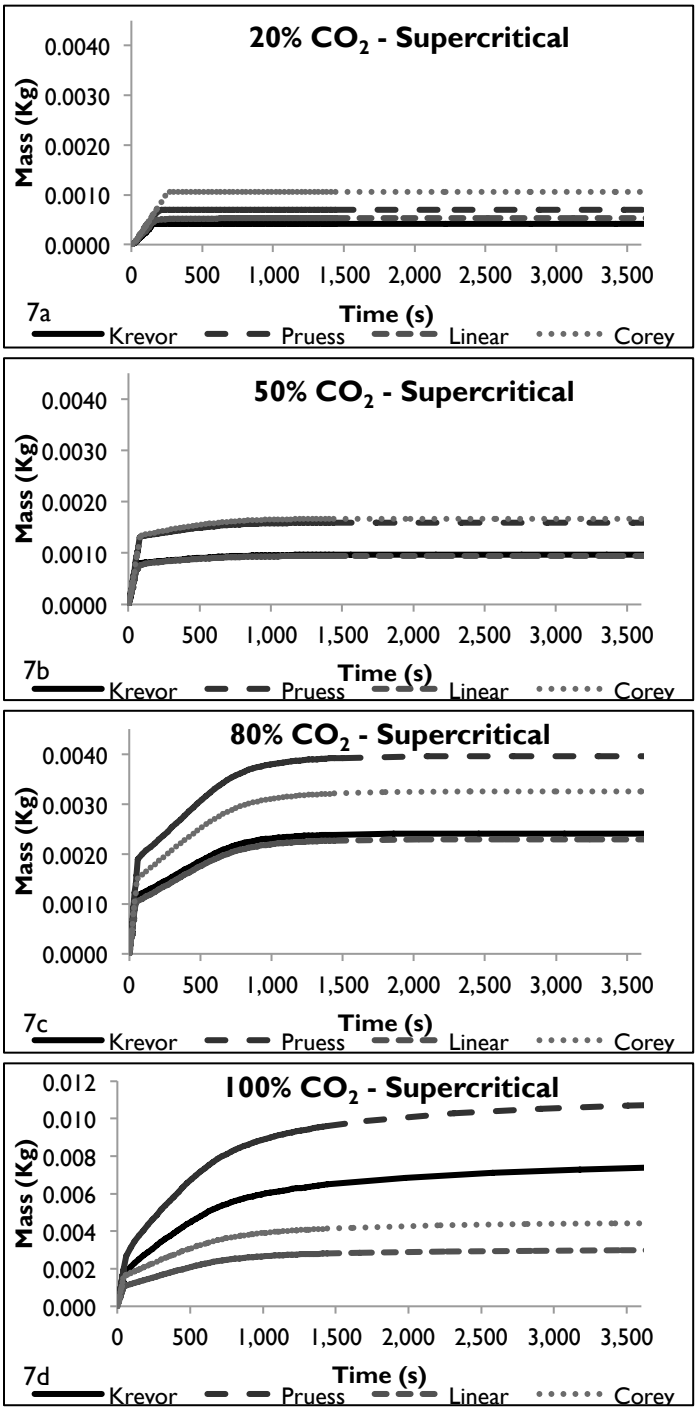

Figure 7. Results of four of the Navajo sandstone core simulations showing the predicted mass of supercritical CO_2 in place for each relative permeability curve. 7a shows the 20% CO_2/80% H_2O simulation, 7b shows the 50% CO_2/50% H_2O simulation, 7c shows the 80% CO_2/20% H_2O simulation, and 7d shows the 100% CO_2 simulation.

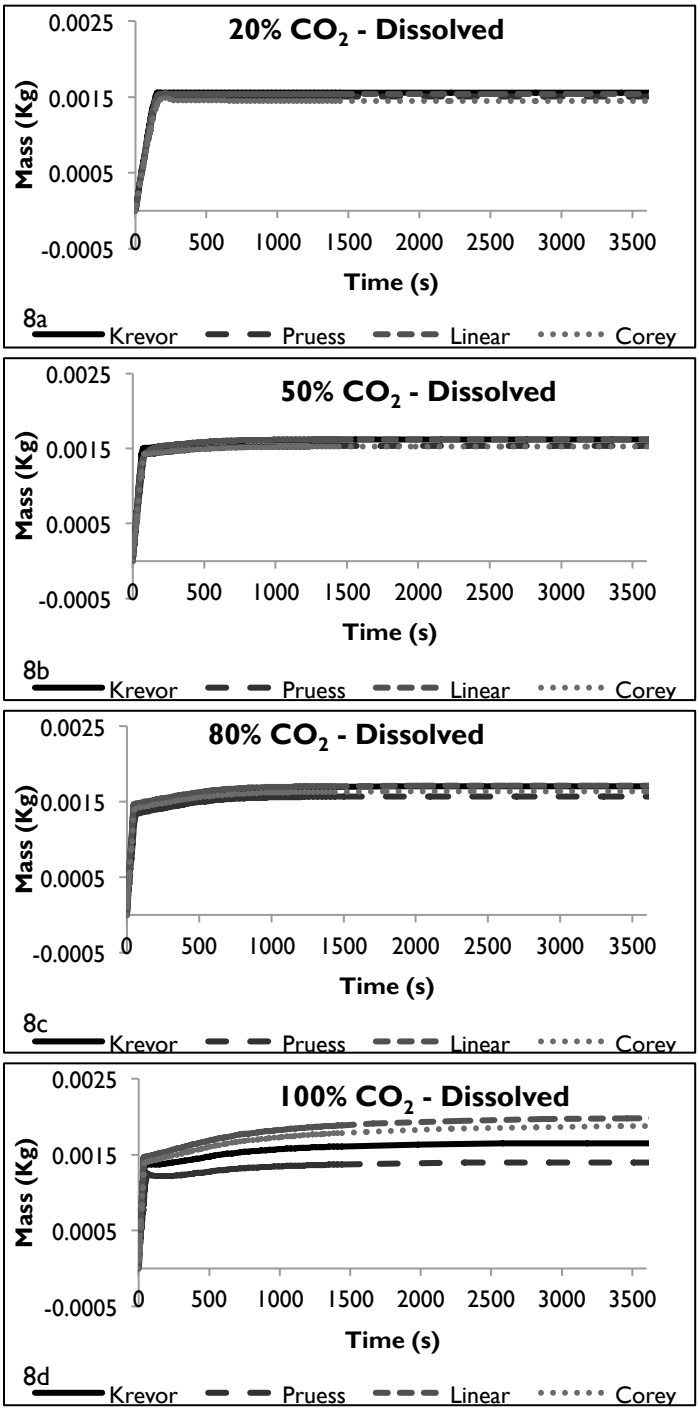

Figure 8. Results of four of the Navajo sandstone simulations showing predicted mass of dissolved CO_2 phase in place for each relative permeability curve. 8a shows the 20% CO_2/80% H_2O simulation, 8b shows the 50% CO_2/50% H_2O simulation, 8c shows the 80% CO_2/20% H_2O simulation, and Fig. 8d shows the 100% CO_2 simulation.

Table 6. Total amount of supercritical and dissolved CO_2 predicted in the Berea Sandstone core model by each of the relative permeability curves.

	20% fractional flow		50% fractional flow	
	Supercritical (g)	Dissolved (g)	Supercritical (g)	Dissolved (g)
Krevor	2.521	1.777	6.080	1.826
Pruess	2.831	1.744	6.148	1.823
Linear	0.646	1.877	1.150	1.983
Corey	1.327	1.768	2.180	1.850
	80% fractional flow		100% fractional flow	
	Supercritical (g)	Dissolved (g)	Supercritical (g)	Dissolved (g)
Krevor	9.717	1.915	26.883	0.927
Pruess	9.178	1.956	24.761	1.090
Linear	2.831	2.089	3.787	2.433
Corey	4.303	1.971	5.968	2.268

Table 7. Total amount of supercritical and dissolved CO_2 predicted in the Navajo Sandstone core model by each of the relative permeability curves.

	20% fractional flow		50% fractional flow	
	Supercritical (g)	Dissolved (g)	Supercritical (g)	Dissolved (g)
Krevor	0.421	1.553	0.967	1.619
Pruess	0.695	1.509	1.593	1.534
Linear	0.528	1.535	0.943	1.622
Corey	1.060	1.450	1.668	1.527
	80% fractional flow		100% fractional flow	
	Supercritical (g)	Dissolved (g)	Supercritical (g)	Dissolved (g)
Krevor	2.411	1.702	8.544	1.577
Pruess	3.962	1.572	11.319	1.362
Linear	2.295	1.711	3.014	1.997
Corey	3.249	1.635	4.452	1.888

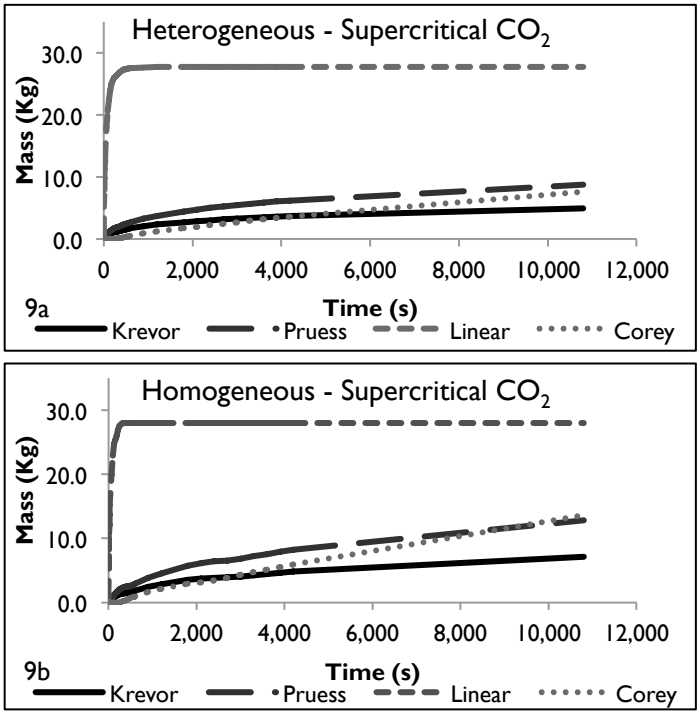

Figure 9. Results of the 10kPa Navajo sandstone bedform model simulations showing the predicted mass of supercritical CO_2 in place for each of the relative permeability curves used in the heterogeneous (9a) and homogeneous (9b) models.

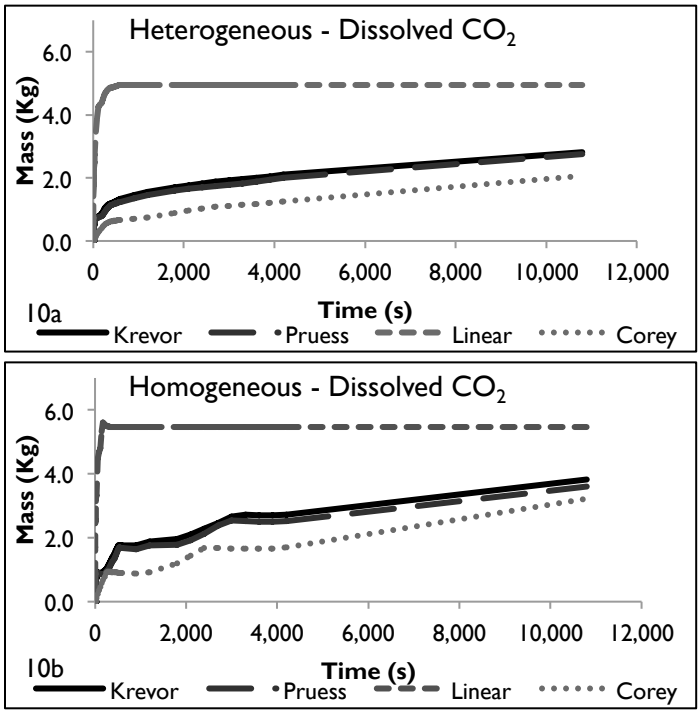

Figure 10. Results of the 10kPa Navajo sandstone bedform model simulations showing the predicted mass of dissolved phase CO_2 in place for each of the relative permeability curves used in the heterogeneous (10a) and homogeneous (10b) models.

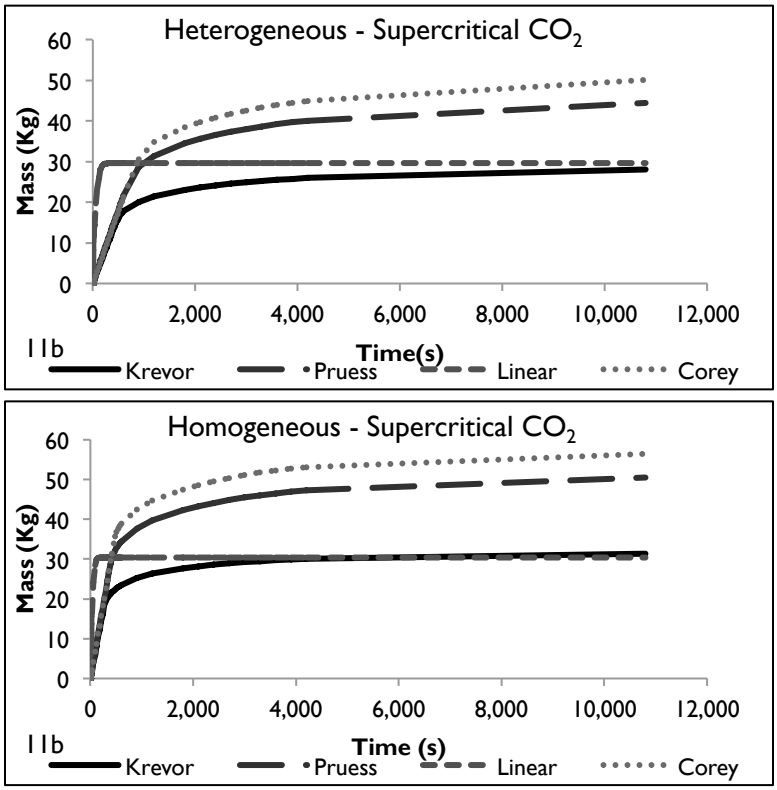

Figure 11. Results of the 100kPa Navajo Sandstone bedform model simulations showing the predicted mass supercritical of CO_2 in place for each of the relative permeability curves used in the heterogeneous (9a) and homogeneous (9b) models.

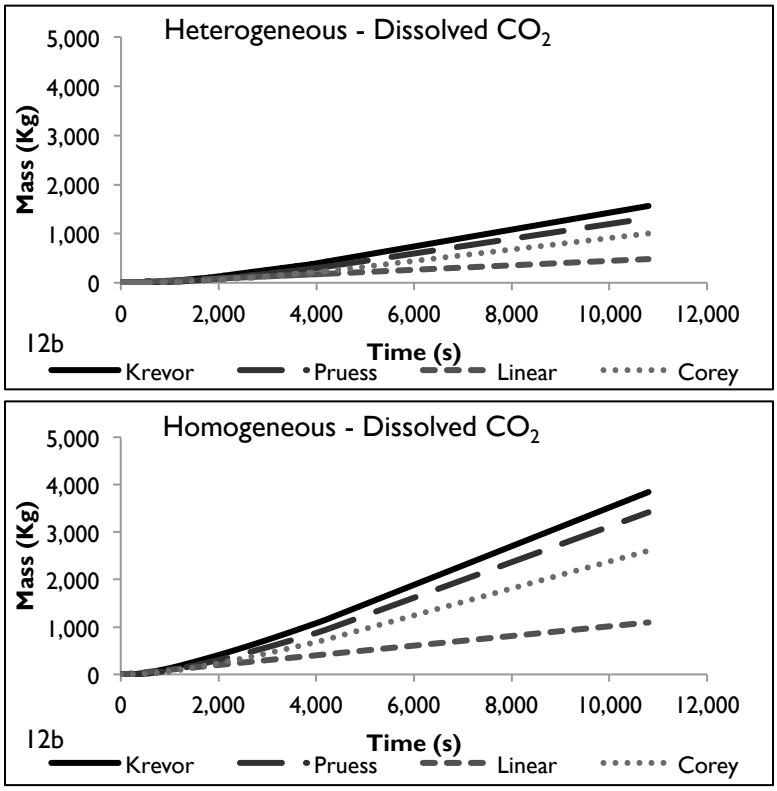

Figure 12. Results of the 100kPa Navajo sandstone bedform model simulations showing the predicted mass dissolved phase of CO_2 in place for each of the relative permeability curves used in the heterogeneous (10a) and homogeneous (10b) models.

Table 8. Total amount of supercritical and dissolved CO_2 predicted in the Navajo Sandstone core model by each of the relative permeability curves.

Heterogeneous Model				
	10kPa		100kPa	
	Supercritical (Kg)	Dissolved (Kg)	Supercritical (Kg)	Dissolved (Kg)
Krevor	4.91	2.81	28.10	1569.51
Pruess	8.72	2.75	44.44	1322.53
Linear	27.72	4.95	29.61	484.30
Corey	7.61	2.07	50.19	999.20
Homogeneous Model				
	10kPa		100kPa	
	Supercritical (Kg)	Dissolved (Kg)	Supercritical (Kg)	Dissolved (Kg)
Krevor	7.17	3.83	31.41	3846.63
Pruess	12.84	3.61	50.53	3419.59
Linear	28.02	5.47	30.42	1095.99
Corey	13.68	3.23	56.47	2608.55

CHAPTER 5

CONCLUSION

The results of this study suggested that the choice of relative permeability function and the parameters used in that function can have a huge impact on predicted CO_2 plume migrations, phase behavior, and storage capacity. As seen with the linear curve, the difference in predicted mass of supercritical CO_2 can be as large as 460% compared to the "base case" Krevor curve. Experimentally derived relative permeability curves for the target reservoir are essential for getting accurate predictions of the amount of CO_2 present and phase behavior. This finding has cast some doubt on the accuracy of models using generalized relative permeability curves to forecast storage capacity and plume behavior in CO_2 sequestration sites. Using a general curve, like the linear function, could lead to a large disparity in predictions for a particular formation. For studies of potential sequestration sites, having a measured relative permeability curve is essential for accurate model predictions.

Our study has indicated that in certain circumstances the dissolved CO_2 phase is sensitive to the relative permeability curve used. Specifically, the linear curve used in the Navajo bedform models exhibits this sensitivity. It could be due possibly to insufficient time for dissolution in the brine caused by the rapid movement of supercritical CO_2 through the model. All models did indicate that the choice of relative permeability curve used has an impact on both supercritical and dissolved phase behavior and total storage capacity. Accurate relative permeability curves for the material being studied are

essential for good predictions of CO_2 storage capacity, phase behavior, and plume movement.

Another important finding was that using an experimentally derived curve for one material, Berea sandstone in our case, as a proxy for a different material, Navajo sandstone, yields completely different CO_2 plume behavior and predicted mass. This gives weight to the idea that unless there are good measured relative permeability curves for the particular formation being studied it is preferred to use generic curves instead of relating curves from different rock types.

One finding that was somewhat surprising was that lower permeability lithofacies within what is normally thought of as a homogeneous medium, as the Navajo sandstone is, can act as an effective seal against the movement of CO_2 under certain relative permeability curves and pressure regimes. This result was observed only in the Navajo sandstone bedform model simulations and not in any of the core flood simulations. It highlights the finding that using the wrong function or parameters can lead to predictions of CO_2 behavior that may not be indicative of what is seen in the field. In the case of the Navajo sandstone bedform model simulations, using the linear curve causes the supercritical CO_2 to reach a saturation plateau while the Krevor, Pruess, and Corey curves trap the CO_2 under the lower permeability wind ripple lamina lithofacies until the end of the simulations.

This study has shown how critical it is to understand the relative permeability of the reservoir rock in question. Having a relative permeability curve derived from experimental data on the rock unit under study will greatly increase the accuracy of the model's predictions of total storage capacity and plume movement as well as CO_2 phase behavior.

To summarize the important findings of our study:

1. Choice of relative permeability function and parameters can have a significant impact on predicted CO_2 plume migration, phase behavior, and storage capacity.

2. Using an experimentally derived relative permeability function and parameters from one material as a proxy for a different material can yield results worse than if a generic function and parameters were used.

3. Under certain conditions, the relative permeability curve used can cause lower permeability lithofacies to act as effective seals to CO_2 movement in reservoir units that would otherwise be considered homogeneous.

REFERENCES

Allen, J., Lee, S.-Y., Potter, S.: Construction of a 3D Geologic Model of the Aeolian Jurassic Navajo Sandstone in Central Utah for the Evaluation of CO2 Sequestration. In. Utah Geological Survey, (2011)

Bielinski, A.: Numerical simulation of CO2 sequestration in geological formations. Inst. für Wasserbau, (2006)

Chidsey, T.C., Chamberlain, L.: Gordon Creek. In, vol. 22. Utah Geological Survey, Salt Lake City, (1996)

Corey, A.T.: The interrelation between gas and oil relative permeabilities. Producers Monthly **19**(1), 38-41 (1954)

Doughty, C., Pruess, K.: Modeling Supercritical Carbon Dioxide in Heterogeneous Porous Media. Vadose Zone Journal **3**, 837-847 (2004)

Doughty, C., Pruess, K., Benson, S.M., Hovorka, S.D., Knox, P.R., Green, C.T.: Capacity investigation of brine-bearing sands of the Frio Formation for geologic sequestration of CO2. In: Proceedings of First National Conference on Carbon Sequestration 2001, pp. 14-17

Hood, J.W., Patterson, D.J.: Bedrock Aquifers in the Northern San Rafael Swell Area, Utah, with Special Emphasis on the Navajo Sandstone. In: Technical Publication No. 78. United States Geological Survey, Salt Lake City, (1984)

Krevor, S.C.M., Pini, R., Zuo, L., Benson, S.M.: Relative permeability and trapping of CO2 and water in sandstone rocks at reservoir conditions. Water Resources Research **48**(W02532) (2012). doi:10.1029/2011WR010859

Kumar, A., Noh, M., Pope, G., Sepehrnoori, K., Bryant, S., Lake, L.: Reservoir simulation of CO2 storage in deep saline aquifers. In: SPE/DOE Symposium on Improved Oil Recovery 2004

Lu, C., Lee, S.-Y., Han, W.S., McPherson, B.J., Lichtner, P.C.: Comments on "Abrupt-Interface Solution for Carbon dioxide Injection into Porous Media" by M. Dentz and D. Tartakovsky. Transport in Porousd Media **79**, 29-37 (2009). doi:10.1007/s11242-009-9362-9

Muller, N.: Supercritical CO2-Brine Relative Permeability Experiments in Reservoir Rocks - Literature Review and Recomendations. Transport in Porousd Media **87**, 367-383 (2011). doi:10.1007/s11242-010-9689-2

Pruess, K., Oldenburg, C., Moridis, G.: TOUGH2 User's Guide, Version 2.0. In. Earth Sciencees Division, Lawrence Berkeley National Laboratory, University of California, Berkeley, (1999)

Pruess, K., Xu, T., Apps, J., Garcia, J.: Numerical modeling of aquifer disposal of CO2. Spe Journal **8**(1), 49-60 (2003)

White, S.P., Allis, R.G., Moore, J., Chidsey, T., Morgan, C., Gwynn, W., Adams, M.: Simulation of reactive transport of injected CO2 on the Colorado Plateau, Utah, USA. Chemical Geology **217**, 387-406 (2005)

White, S.P., Weir, G.J., Kissling, W.M.: Numerical simulation of CO2 sequestration in natural CO2 reservoirs on the Colorado Plateau. In: Proceedings of First National Conference on Carbon Sequestration, Washington, DC 2001

Xu, T., Apps, J.A., Pruess, K.: Numerical simulation of CO2 disposal by mineral trapping in deep aquifers. Applied geochemistry **19**(6), 917-936 (2004)

Xu, T., Apps, J.A., Pruess, K.: Mineral sequestration of carbon dioxide in a sandstone–shale system. Chemical Geology **217**(3), 295-318 (2005)